



LAWRENCE
LIVERMORE
NATIONAL
LABORATORY

Application of an EMCCD Camera for Calibration of Hard X-Ray Telescopes

J. K. Vogel, M. J. Pivovarov, V. V. Nagarkar, H.
Kudrolli, K. Kruse Madsen, J. E. Koglin, F. E.
Christensen, N. F. Brejnholt

November 11, 2011

IEEE NSS MIC 2011
Valencia, Spain
October 23, 2011 through October 29, 2011

Disclaimer

This document was prepared as an account of work sponsored by an agency of the United States government. Neither the United States government nor Lawrence Livermore National Security, LLC, nor any of their employees makes any warranty, expressed or implied, or assumes any legal liability or responsibility for the accuracy, completeness, or usefulness of any information, apparatus, product, or process disclosed, or represents that its use would not infringe privately owned rights. Reference herein to any specific commercial product, process, or service by trade name, trademark, manufacturer, or otherwise does not necessarily constitute or imply its endorsement, recommendation, or favoring by the United States government or Lawrence Livermore National Security, LLC. The views and opinions of authors expressed herein do not necessarily state or reflect those of the United States government or Lawrence Livermore National Security, LLC, and shall not be used for advertising or product endorsement purposes.

Application of an EMCCD Camera for Calibration of Hard X-Ray Telescopes

Julia K. Vogel, Michael J. Pivovarov, Vivek V. Nagarkar, Haris Kudrolli, Kristin Kruse Madsen, Jason E. Koglin, Finn E. Christensen, and Nicolai F. Brehnholt

Abstract—Recent technological innovations now make it feasible to construct hard x-ray telescopes for space-based astronomical missions. Focusing optics are capable of improving the sensitivity in the energy range above 10 keV by orders of magnitude compared to previously used instruments. The last decade has seen focusing optics developed for balloon experiments [1] and they will soon be implemented in approved space missions such as the Nuclear Spectroscopic Telescope Array (NuSTAR) [2] and ASTRO-H [3]. The full characterization of x-ray optics for astrophysical and solar imaging missions, including measurement of the point spread function (PSF) as well as scattering and reflectivity properties of substrate coatings, requires a very high spatial resolution, high sensitivity, photon counting and energy discriminating, large area detector. Novel back-thinned Electron Multiplying Charge-Coupled Devices (EMCCDs) [4] are highly suitable detectors for ground-based calibrations. Their chip can be optically coupled to a microcolumnar CsI(Tl) scintillator [5] via a fiberoptic taper. Not only does this device exhibit low noise and high spatial resolution inherent to CCDs, but the EMCCD is also able to handle high frame rates due to its controllable internal gain. Additionally, thick CsI(Tl) yields high detection efficiency for x-rays [6]. This type of detector has already proven to be a unique device very suitable for calibrations in astrophysics: such a camera was used to support the characterization of the performance for all NuSTAR optics [7]–[9]. Further optimization will enable similar cameras to be improved and used to calibrate x-ray telescopes for future space missions.

In this paper, we discuss the advantages of using an EMCCD to calibrate hard x-ray optics. We will illustrate the promising features of this detector solution using examples of data obtained during the ground calibration of the NuSTAR telescopes performed at Columbia University during 2010/2011. Finally, we give an outlook on ongoing development and optimizations, such as the use of single photon counting mode to enhance spectral resolution.

Index Terms—EMCCD, NuSTAR, hard x-ray mission, hard x-ray detectors, calibration, scintillator, x-ray detectors.

I. INTRODUCTION

With the hard x-ray ($E \approx 10 - 100$ keV) universe still harboring many mysteries waiting to be explained, the technological advances over the last decade in the development of x-ray focusing optics have been eagerly anticipated. In contrast to previously employed devices like collimators and coded-mask cameras, focusing optics provide high sensitivity in the hard x-ray range above 10 keV. Increases by up to a factor of 100 can be achieved using this novel technology over conventional devices. In recent years, such focusing optics were developed for balloon experiments [1] and will be implemented in approved space missions such as the Nuclear Spectroscopic Telescope Array (NuSTAR [2]) and ASTRO-H [3], as well as onboard of proposed experiments such as

the New Hard X-Ray Mission (NHXM [10]). Calibration of the focusing components is crucial, on the ground as well as in orbit. We will discuss the possibility of using a novel EMCCD detector for ground calibration of hard x-ray satellite missions. This device has already been tested and successfully used in characterizing NuSTAR flight and flight spare telescopes and we will use these results to demonstrate the vast potential of the EMCCD for calibrating hard x-ray space missions.

II. THE EMCCD DETECTOR

Novel back-thinned Electron Multiplying Charge-Coupled Devices (EMCCDs, see Figure 1) are suitable detectors for hard x-ray measurements. Their chip can be optically cou-



Fig. 1. The Andor iXon EMCCD camera developed at RMD ([4], [5]). A 1:1 fiberoptic plug is permanently attached to the chip. In the left part of the image an additional, detachable 3:1 fiberoptic taper is shown.

pled to a microcolumnar CsI(Tl) scintillator (see Figure 2) via a fiberoptic taper. A 1:1 fiberoptic plug is permanently installed to connect the chip and the scintillator material. If an observation requires a larger sensitive detector area, an additional, detachable 3:1 taper can be installed. This increases the detector area by a factor of 9 but decreases the sensitivity of the camera due to the optical light loss in the fiber optic taper.

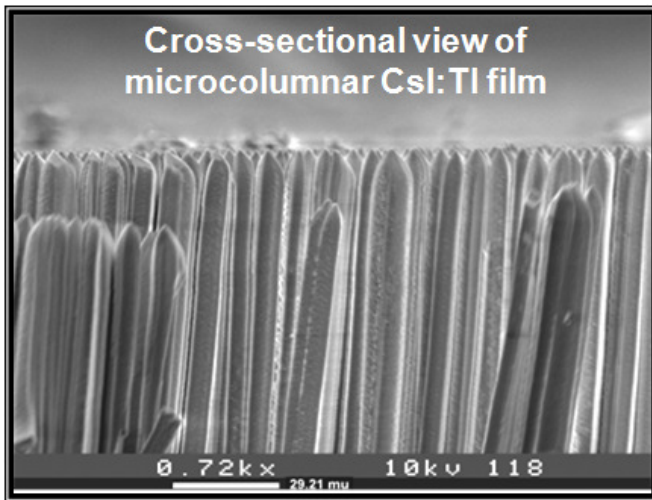


Fig. 2. Cross-sectional SEM view of microcolumnar CsI(Tl) film which has been deposited on a suitable substrate [6]. The column diameter is on average about $10 \mu\text{m}$.

The advantages of such an EMCCD detector system are multifold. It exhibits both the low noise and high spatial resolution typical for CCDs, but in addition to this, the EMCCD is also able to handle high frame rates due to the fact that its internal gain is controllable. Thus it combines the advantages of a conventional CCD detector with the high sensitivity of an avalanche photo diode (APD).

A further advantage of this detector system is the use of a high-density and high light-yield scintillator which exhibits a fast decay time and can be produced as a film by vapor deposition onto graphite or other suitable substrates. Thick CsI(Tl) in combination with an EMCCD yields high detection efficiency for x-rays.

The microcolumnar structure of the scintillator makes use of the principle of total internal reflection to guide the scintillation light produced by incident x-rays to the EMCCD chip. In this way a significant spread of the created scintillation light is prevented. The application of this type of detector in characterizing the response of hard x-ray telescopes thus yields excellent spatial resolution.

All these advantages, in combination with the robust turn-key technology present, make this detector a prime candidate for characterizing future hard x-ray space missions. Further optimization of this technology is underway and will lead to new improvements.

III. THE NUSTAR MISSION

In this section, we briefly introduce the main features of the optics system used for the NuSTAR mission, since we will use examples of the calibration measurements for these optics to demonstrate the performance of the proposed detector system.

NuSTAR is one of NASA's Small Explorer (SMEX) missions scheduled to launch in Spring 2012. The satellite features two coated multilayer (ML) optics with CdZnTe detectors in the focal plane and is sensitive in the energy band of 5-

80 keV. The application of ML x-ray mirror optics ([7], [11]) enables the state-of-the-art experiment to increase its sensitivity by a factor of 50-100 in the hard x-ray regime as compared to previous missions. In the case of NuSTAR the telescopes are conical approximations to Wolter-I telescopes. The good sub-arcminute resolution of NuSTAR paired with its excellent spectral resolution will allow for groundbreaking studies in astrophysics such as the study of supermassive black holes, compact objects in the Galaxy and supernovae remnants. Detailed calibrations on-ground and in-orbit will be essential to all science data interpretation.

For further details on the NuSTAR apparatus and its science mission, the reader is referred to Refs. [2], [7], [8] and [11].

IV. APPLICATION OF THE EMCCD FOR NUSTAR GROUND CALIBRATION

From October 2010 to March 2011 all three NuSTAR telescopes (two flight optics and one flight spare) were calibrated at the Rainwater Memorial Calibration Facility (RaM-CaF [12]). Before characterizing flight telescopes, we verified the linear response of the EMCCD camera by increasing the source current of the Comet XRS-100 x-ray system installed at the calibration facility. We cross-calibrated with a high-purity Germanium detector which was also used for optics characterization.

The camera was operated in integration mode when measuring the optics response of all three NuSTAR telescopes. For measurements on the flight telescopes, the 3:1 taper and a CsI(Tl) scintillator were used to cover a larger fraction of the optics response. In order to study the full extent of the image for all NuSTAR optics we mounted the detector on a motorized stage and scanned the telescope output in the plane orthogonal to the beam axis.

The EMCCD camera played a crucial role in the ground calibration of the two x-ray telescopes built to fly on NuSTAR as well as in the characterization of the flight spare optic. More precisely, the following procedures were performed using this detector:

- Installation and alignment of telescopes in the beamline of the RaM-CaF facility.
- Characterization of point-spread function (PSF) on-axis and off-axis, in discrete energy bands and the full range spectrum of the calibration facility.
- Validation of ray-trace simulations with respect to effects of finite source distance and the use of a diverging source, as well as the influence of gravity, figure, and finish.
- Characterization of RaM-CaF features, such as slit size and position, monitoring through-holes in the experimental setup, etc.

The efficiency, effectiveness and power of using a silicon solid-state detector coupled to a scintillating material for development and calibration of x-ray optics has been fully validated with the data acquired as part of the NuSTAR ground calibration campaign.

In the following subsections we will discuss each task in more detail.

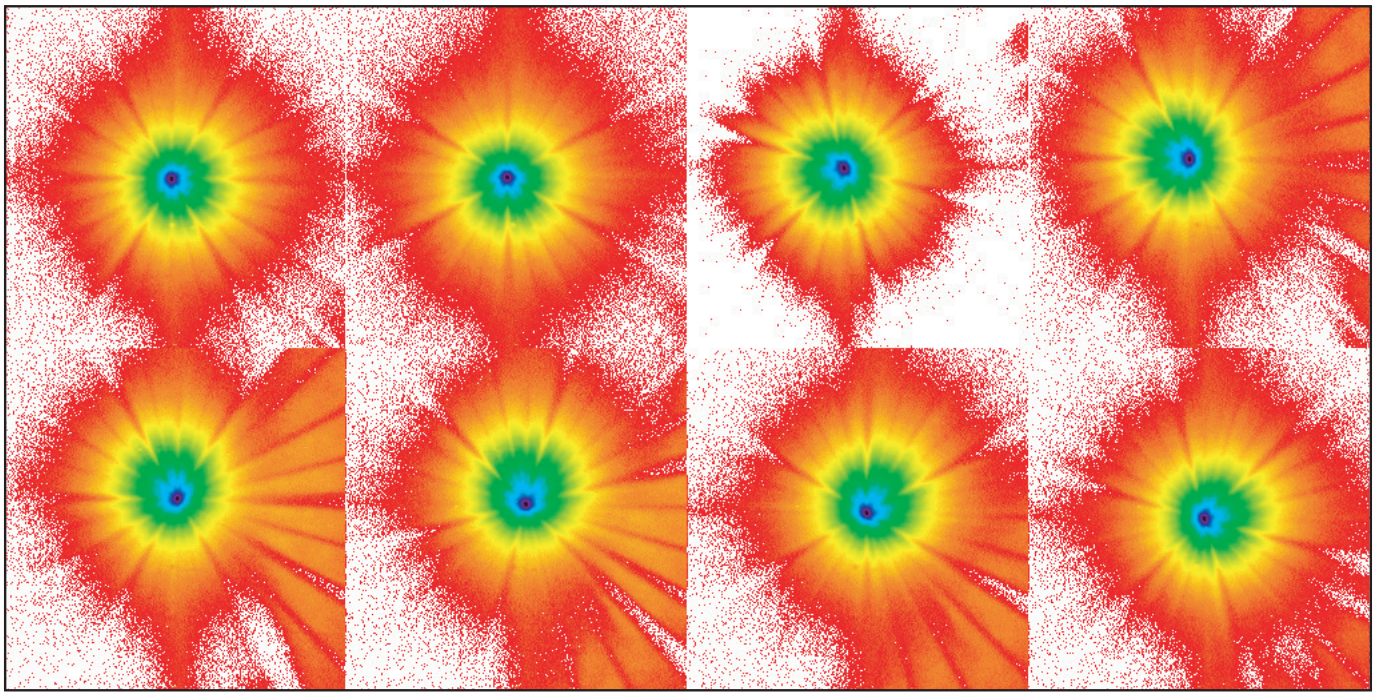


Fig. 3. Point spread function (PSF) data acquired when rotating the telescope in increments of 45° about the axis. The shift of the centroid position in these images indicates that the telescope axis is misaligned with respect to the facility axis. After adjusting the telescope position, subsequent data confirmed proper alignment of the telescope to the calibration facility axis. Note that the observable asymmetry in the images results from a combination of two effects: the influence of gravity and a bend of the optics due to stress induced by tightened mounting struts of the telescope support.

A. Installment and Alignment

In order to precisely locate and move the NuSTAR optics during calibration, each telescope was mounted to a large rotation stage. A series of adjustable struts kept the optic in place and prevented unwanted movement. The first alignment procedure is intended to provide an initial alignment of the x-ray axis of the telescope to the x-ray axis of the calibration facility, using visible light surveying techniques and fiducial alignment features. The proxy for the x-ray axis of RamCaF were two sets of cross-hairs that consist of two perpendicular wires. The proxy for the x-ray axis of the telescopes were two pinholes located at the front and back of the cylindrical support on which the x-ray telescope was built. The position of the optic was changed (by adjusting both the struts and the location of the rotation stage) until the pinholes were co-located to the cross-hairs.

To verify this initial alignment, the optic was illuminated with x-rays and the centroid of the pinhole was recorded on the EMCCD as a function of azimuthal (or roll angle) position within the large rotation stage. The results obtained applying this technique needed to be validated *in situ* and improved if necessary. Thus a rapid and effective collection of x-ray data was an important requirement. The calibration specification for precession of the rotation of the optic (provided by the large rotation stage) with respect to the calibration facility was less than $10''$ radial offset. Using the EMCCD, images of the PSF at various roll angles, i.e. different azimuth positions of the optic, were acquired. The centroid position for each PSF image

(see Figure 3) can then be determined and used to quantify the amount of precession. In this specific example (see Figure 4), the recorded data showed that the initial alignment (dotted line, $18''$ radial precession) did not meet the requirement. After additional adjustments were made, the PSF measurements at different roll positions were repeated (dashed line, $8''$ radial precession) and used to verify that the precession tolerance met specifications. The two data sets show that after the re-adjustment, the alignment was improved and fully met the NuSTAR calibration requirements.

B. Point Spread Function

Measuring the point spread function (PSF) of the NuSTAR telescopes was one of the primary goals of the optics calibration campaign and the major task of the EMCCD detector. This camera made it possible to study the evolution of the PSF as a function of both off-axis position and energy in real time. During all calibration measurements at RamCaF the EMCCD was operated in integration mode rather than single photon counting mode due to a tight time schedule. In order to observe energy dependencies, we created broad spectral bands by precisely matching the end-point energy of the x-ray source with carefully chosen filters. A total of four energy bands were studied, i.e. a broad band and three narrow bands of about 15 keV width: x

- Full broad-band bremsstrahlung spectrum of the source covering energies from about 15-100 keV with target material lines at the higher end of the spectrum (see Figure 5).

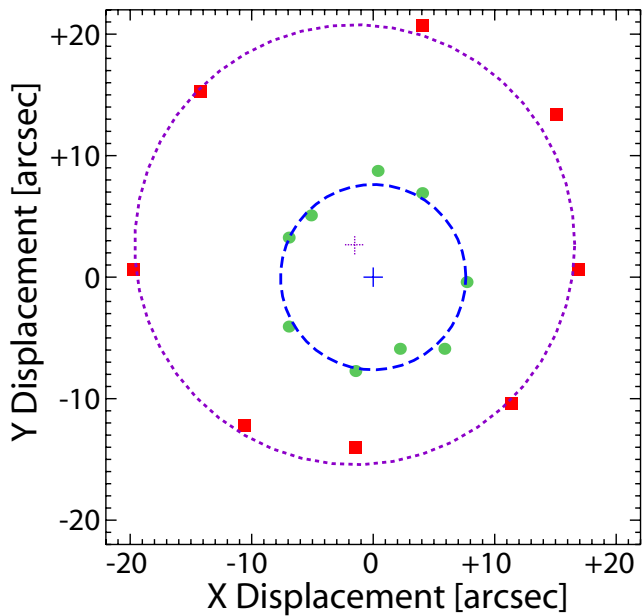


Fig. 4. Relative centroid positions of the PSF as a function of various azimuth positions. While the red squares and purple dotted circle indicate the initial position, the green circles and blue dashed circle demonstrate the improved alignment after adjustments. The circles represent the magnitude of the precession between the rotation axis of the large stage to which the x-ray telescope is mounted and the facility x-ray axis. The crosses indicate the center points of the precession circles and any difference from (0,0) indicates an additional offset of the two x-ray axes. Linear dimensions were converted to angular displacement using a plate scale of $1 \text{ mm} = 19.1''$.

- Narrow, near Gaussian-shaped bands around 30, 55 and 70 keV.

In order to additionally determine the off-axis response of the telescopes, the pitch and yaw of the optics' mounting were carefully adjusted.

It is important to mention that the measured performance on ground will necessarily differ from the expected performance in space. This is due to several factors: the distance between the x-ray source and the telescope is finite, the beam is divergent and the stray-light-limiting apertures that will be present in the satellite are absent on ground. Therefore the PSF as observed on the ground will include additional features which will not be observable on orbit. The most important "on

ground" effect are "ghost rays" resulting from single reflected light, i.e. photons that have only been reflected off one single mirror surface. Double reflected photons, on the other hand, are properly focused and form the core of the PSF. Even though ghost rays are unwanted events on orbit, they prove to be very useful during ground calibrations since they can be used to identify figure errors in individual mirror segments.

During NuSTAR calibrations the telescopes have been illuminated in different ways. If the entire telescope aperture was flooded with x-rays, this will be commonly referred to as full-flood illumination, while the term subgroup illumination is used to express that only limited regions, i.e. subgroups of the optic, were open to x-rays due to the use of lead plates with narrow, annular openings.

An example of such a sub-group illumination measurement can be found in Figure 6. The image was obtained by systematically moving the camera in the horizontal direction

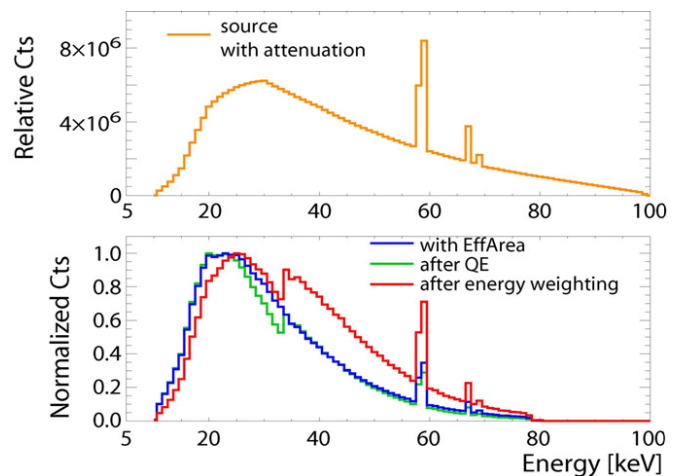


Fig. 5. Full x-ray spectrum of the Comet XRS-100 x-ray system at RaMCaF. Top: Full source spectrum including attenuation in air is shown. Bottom: The blue spectrum indicates the influence of the effective area of the NuSTAR telescope on the incoming source spectrum. Applying the quantum efficiency of the detector in addition to the optics effective area yields the green curve. If furthermore the energy weighting is taken into account the red and final expected spectrum is obtained. By energy weighting we refer to the effect that an 80 keV photon will produce four times the scintillation light produced by a 20 keV photon.

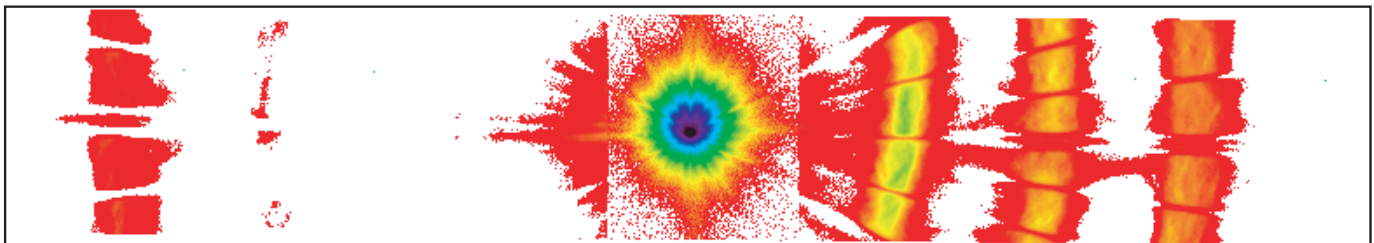


Fig. 6. Telescope response for source $2''$ off-axis. Image is a composite of data acquired at seven different horizontal positions. The central core shows the properly focused light and is the true PSF. The vertical streaks are an artifact and result from events registered during the readout of the CCD chip. The vertical bands to the left and right of the core (three to the right, two to the left) result from single reflected light and are referred to as ghost-rays. The apparent vertical bands are in reality annular rings, that extended above and below the area of the detector. These rings result from the use of aperture limits used to illuminate specific regions of the telescope.

in seven unique position, because the ghost rays extend well beyond the field of view of the EMCCD chip (about 25 mm × 25 mm). The resulting mosaic image was exposure corrected and yields a total image that is approximately 150 mm wide.

In order to obtain the entire PSF, the optics were systematically rotated about their optical axis and horizontal raster-scans were acquired at each rotation position. The images of these different positions were then assembled and exposure-corrected. For subgroup illumination of the full optic (NuSTAR flight module 1, FM1), 70 images of EMCCD data were acquired. For full-flood illumination (NuSTAR flight module 2, FM2), 90 exposures were used to create a view of the full optics. The resulting mosaic images are shown in Figure 7 and Figure 8, respectively. Note that the color scale is logarithmic in these plots, i.e. ghost rays are very faint compared to the core image. In both images the shadow effect of the telescope support structure, commonly referred to as a spider, as well as individual graphite spacers can be identified. Figure 7 depicts the illumination of 4 subgroups. In the full flood illumination (Figure 8), the change from 60° azimuthal sectors (inner mirror shells) to 30° sectors (outer shells) is observable.

First results for the half power diameter (HPD) of the NuSTAR telescopes have been determined and yield a value of about 52'' which meets the NuSTAR sensitivity requirements [9].

C. Validation of Raytrace Simulations

It is important for any ground calibration of an x-ray telescope to account for the differences between astrophysical and facility sources. While astrophysical sources provide parallel

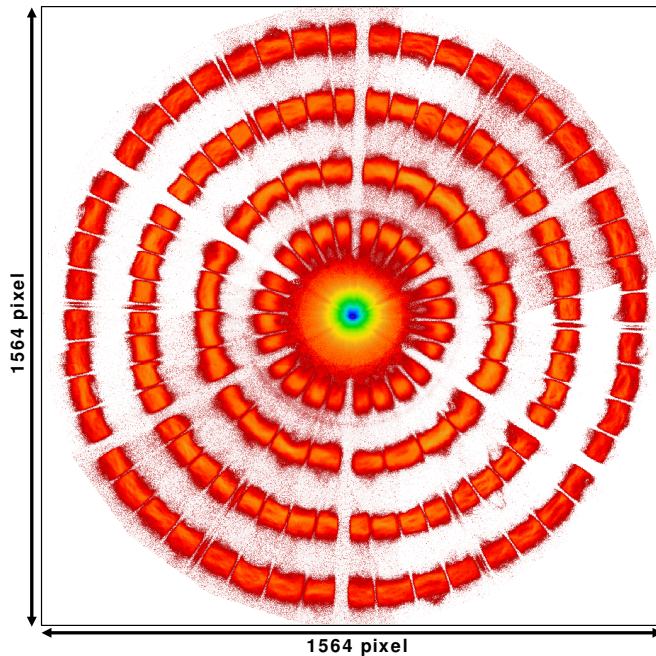


Fig. 7. Illumination of subgroups for NuSTAR's FM1 optic, obtained by mosaic imaging with the EMCCD camera. Four subgroups were illuminated here. The spider structure of the optics support is visible in the logarithmic color scale display.

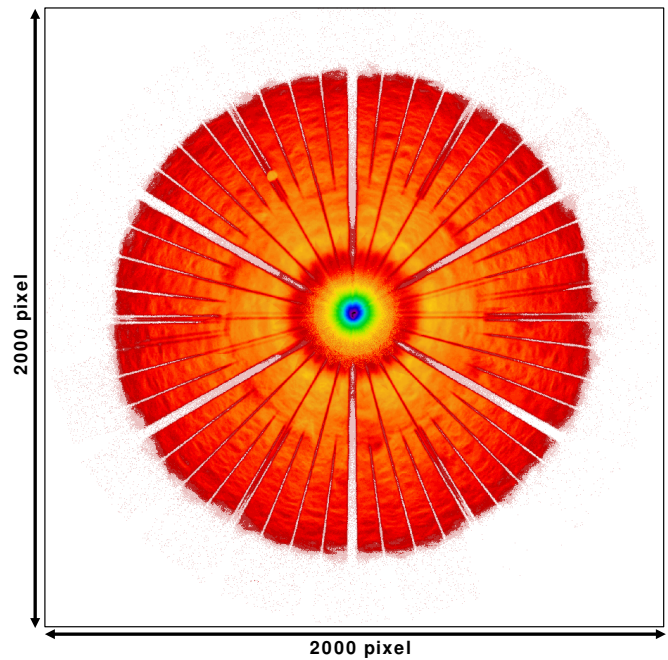


Fig. 8. Full flood illumination of NuSTAR's FM2 optic, obtained by mosaic imaging with the EMCCD camera. Both the spider structure and the graphite spacers can be observed in this image. Note the logarithmic color scale used.

light that uniformly fills the aperture, calibration sources in the laboratory provide diverging light that is spatially extended and may not uniformly fill the aperture nor uniformly illuminate the mirror surfaces. An accurate optics model is required to precisely predict on-orbit performance. The model needs to be able to account for the differences resulting from the distinct sources and must be capable of reliably reproducing the ground calibration results.

The common approach for x-ray telescopes, is to use a Monte Carlo simulation that first generates individual photons and then propagates each photon through the telescope. This technique, which is also referred to as ray-tracing, accounts for various factors, such as finite reflectivity, figure errors, spatial roughness and the influence of support structures. Performance factors (e.g. mirror roughness or obscuration percentages) can either be adjusted to match the calibration data or they can be fixed, based on previous measurements. A detailed discussion of the NuSTAR telescope model and the complete simulator (NuSim) is beyond the scope of this paper. The interested reader is referred to Ref. [13].

To illustrate the usefulness of the EMCCD data to validate such a model, Figure 9 provides an example. Here data obtained at RaMCaF with the EMCCD is compared to one such model. It can be seen that the simulator reproduces the main features of the (off-axis) data set very well. Note that the structure in the central part of the data image will be discussed in the following sections, but is not relevant to the comparison at hand.

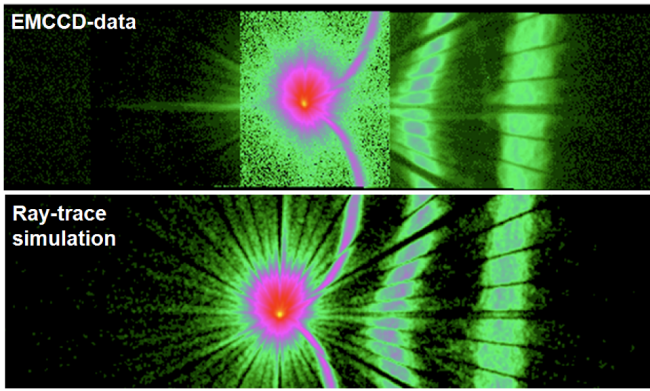


Fig. 9. Comparison between data acquired at RaMCaF with one of the NuSTAR optics using the EMCCD and a Monte Carlo simulation. These data were acquired in an off-axis position to validate the raytrace model.

D. Characterization of Facility Features

A versatile and easy-to-use two-dimensional detector can also be used for another critical task, i.e. a characterization of the x-ray calibration facility itself. While during optics calibration one assumes that both the x-ray source and other equipment are behaving as intended, this can be verified before, during and after the actual measurements by using the EMCCD detector. Once it is mounted on translation stages that allow for movement of the camera over larger ranges, it can be used to map the illumination pattern of the x-rays coming from the source and ensure they have the desired properties. As an example, Figure 10 shows an image that could be used to identify that a drive mechanism had not been retracted and was partially obscuring the entrance aperture. In this instance, imaging with a 2D detector allowed for fast and unambiguous diagnosis of the situation.

V. CHALLENGES OF THE EMCCD DETECTOR SYSTEM

The current detector setup used in testing and calibrating the NuSTAR optics at RaMCaF demonstrated excellent performance and delivered critical results. Its potential for application to future calibration campaigns for hard x-ray telescopes is evident and current work focuses on the advancement of sensitivity at low x-ray energies and in low flux conditions.

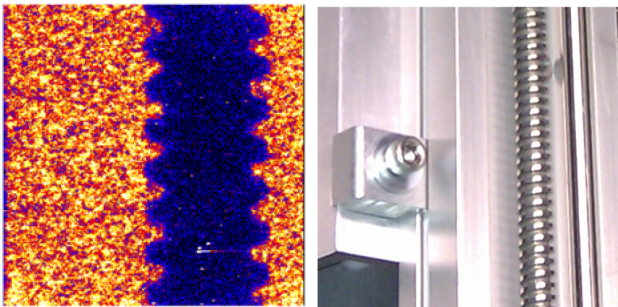


Fig. 10. Left: shadow originating from a drive screw that was not retracted properly and was thus blocking the line of sight for the detector. Right: Photo of the drive screw (right part of image).

Here we will first describe the observed effects, followed in the next section by ongoing efforts to find a solution which includes both software and hardware developments.

During calibrations at RaMCaF, the EMCCD camera was used to calibrate both flight optics of the NuSTAR mission. The focused core image of each x-ray telescope can be fully imaged on the chip of the EMCCD, if a 3:1 taper is used. In order to map the complete optic and study the behavior of the telescope for both double reflected (core of the Point Spread Function) and single reflected photons (wings of the PSF), we scanned a larger area with the EMCCD detector. Due to high intensities in the core and low intensities in the outer regions, various current settings were used to achieve optimal detector performance. When arranging the single images into a complete map of the optics, the images had to be normalized for the intentional variation in x-ray source intensity used during data acquisition.

During this process, we observed a different detector response in the core images, i.e. those frames with very high count rates. Specifically, more events were observed in the “halo” surrounding the tightly-focused core of the PSF. An example of this halo was shown in the top part of Figure 9. The effect under discussion can be observed in the central frame, where the count level immediately around the PSF core seems to be higher than in the neighboring images after adjusting for the fact that this image was taking at lower current settings.

We explored various scenarios to explain this effect, including: Out-of-time-events (OOT; photons interacting in the EMCCD during read-out of the chip), streaking (de-trapping of charge from lattice defect sites in the CCD silicon during transfer), blooming (charge overfilling the well of a single pixel), blurring (due to the spread of the scintillator light) and afterglow (the slow production of scintillator light after the x-ray photons have stopped hitting the scintillator). None of these effects were able to account for the observed phenomena. Most of the above mentioned effects were either present at only the percent level (OOT events, blurring) or could only account for the excess of events in certain regions of the chip (streaking, blooming). Significant contributions of afterglow effects were excluded due to the fact that they would have also been apparent in other situations during data acquisition, e.g. when changing from observing the core to observing the wings. This was not the case.

Closer studies revealed a dependence of the observed effect on the intensity of the incoming radiation. For high photon intensities and non-saturation of the chip, we observed a linear scaling of the event intensity with the source current in both the core and the wings. When the photon intensity was lowered (e.g. by reducing the current in the x-ray tube), this linearity was lost. To illustrate this observation, Figure 11 shows a study of intensity with a broad-band x-ray spectrum (about 20-80 keV). In the top image the intensity for different current settings is shown. The two-dimensional chip was projected onto one coordinate by summing up the intensities for all pixels in one direction in order to simplify visualization. The middle image shows the intensity of each curve expressed as

a percentage of the 5 mA data set. For example, the red curve in this middle figure represents the percentage intensity of the 2 mA curve relative to the 5 mA curve. Since linearity with current is expected, the percentage should be 40%, which is indicated by the red dashed line. The same is shown for both the 1 mA and the 0.5 mA curve with expected levels of 20% and 10%, respectively. It can be seen that while the data from the current of 2 mA scales as expected, for the lower current measurements, the values in the wings quickly drop below the expected percentage. Note that Figure 11 has been corrected for saturation of the core at a current of 5 mA.

Finally the plot at the bottom of Figure 11 shows that we can apply a valid correction, given our explanation of the effect. In this case, we can use the difference between two curves to correct a third one (in this image the 5 mA curve for which the chip was saturated has been corrected). Note that the shown ad-hoc adjustment has only been done for the projected data. In principle this type of correction should be also applicable for the full data set. Thus, all that is left to do to justify a correction of the data based on our studies, is to provide a plausible explanation for the observed effects in the EMCCD. Since the effect is clearly intensity dependent we suggest the following mechanism: in order to detect incoming x-rays with

the EMCCD, enough visible light needs to be produced in the scintillator. Photons at the lower end of our spectrum (around 20 keV) are absorbed shortly after entering the scintillator, and not only will they create a small number of visible photons, but this light will also be spread on the relatively long way to the EMCCD chip. For this reason, low event intensities might not be able to reach above the threshold of the EMCCD. Thus, we expect a non-linear response. At low intensities, no signal is measured. After a certain point, enough x-ray photons are present to create sufficient numbers of scintillator photons that are detectable above the noise threshold of the camera. With increasing count rates, more visible light is produced and—given enough incident photons—some of it will reach the chip, “restoring” linearity. A similar consideration also holds for photons at the upper end of our spectrum (around 80 keV). Although the interaction in the scintillator will take place closer to the chip, i.e. deeper in the scintillator material, only few photons of this energy reach the detector in the first place due to the initial spectrum which favors low energies. The reason for this is the Bremsstrahlung source spectrum as well as the effective area of the telescope, which is higher for lower energies. Thus even though more visible light is produced by a high energy photon as compared to lower energy x-rays, linear behavior can only be observed for x-ray fluxes above a certain level.

In summary, the observed effects can be explained by interactions of the photons in the scintillator, which do not produce enough visible light to cross the threshold of the EMCCD chip and are thus missed by the detector. These effects can be accounted for in the present data set and corrections can be applied. For future use of the detector, such problems can be avoided by either using single photon counting mode or adjusting the scintillator to the observed energies of x-rays when acquiring data in integration mode. This would imply using a thin scintillator for detecting low energy photons and scintillators of increasing thickness for higher energies. Additionally, a scintillator with higher light yield could improve the situation.

Further studies are underway to test further effects that could contribute. Very high countrates and a spread of charge could for example be co-responsible for observed effects in the central frame.

VI. IMPROVING THE EMCCD DETECTOR SYSTEM

A. Hardware improvements

Three major upgrades to the hardware system are envisioned for our future work. One goal will focus on improving the performance of the detector by advancing the EMCCD camera, while the second aim is to enhance the fiber optic bonding to the scintillator. The third envisioned change to the system will be refining the scintillator material itself.

The EMCCD chip employed for future x-ray telescope calibration will be the largest sensor of its kind ever produced. A resolution of one megapixel with a pixel size of $13 \times 13 \mu\text{m}$ is expected. The resulting advantage is that the camera has an increased active area as compared to the present setup,

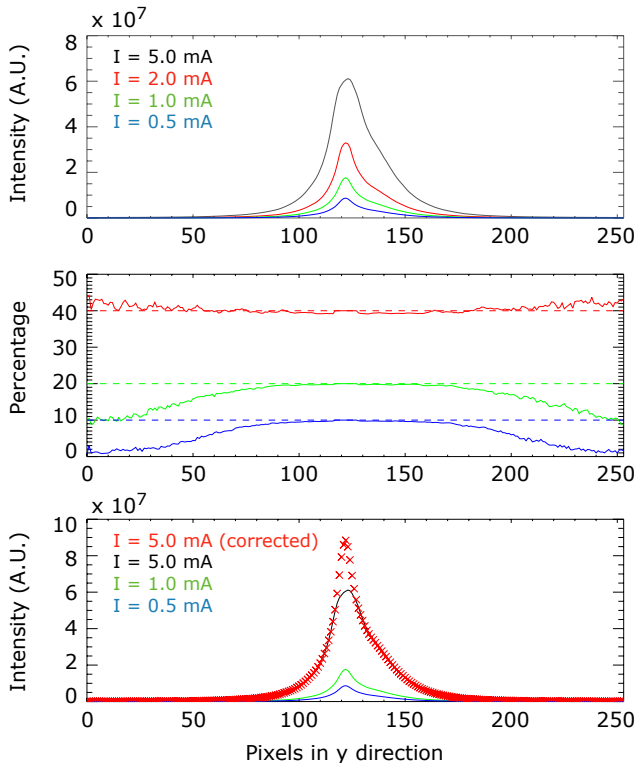


Fig. 11. Top: Intensity projected on y direction. The full energy range is displayed for 4 different current settings of the x-ray source. Note that for the case of the black curve, saturation of the chip was observed. Middle: Percentage of observed intensity as compared to the 5 mA curve in top plot. Linearity with current is expected and the dashed lines indicate the expected level of percentage. Bottom: Applied correction of the 5 mA curve (black) based on a correction matrix obtained from mapping the blue curve (0.5 mA) onto the green curve (1 mA) and adjusting it to fit 5 mA current.

while maintaining the possibility to operate the detector at high frame rates without increasing readout noise. Using a 3:1 fiberoptic taper will enable us to enlarge the active area to $\approx 260\%$ of the camera system currently in use.

The detector used for calibration measurements of NuSTAR consisted of a $450 \mu\text{m}$ thick CsI(Tl) scintillator that was coupled via a fixed 1:1 optical plug and an additional 3:1 fiberoptic taper to the back-thinned EMCCD chip. For the next generation of the device, we will omit the 1:1 plug and will bond the small end of the 3:1 taper directly to the EMCCD chip. Since each interface results in losses of about 10% in spatial resolution and signal, this is a promising way to minimize signal degradation and simultaneously enhance sensitivity and energy resolution.

The third area for improvements is the scintillator. As mentioned in the previous section, due to the use of a relatively thick scintillator, non-linear effects in the detector response were observed. The simple solution here is to use scintillators of varying thickness that are matched to the energy that is being measured, i.e. thin materials for low energy x-rays and thicker ones for higher energies. Additionally, improvement can come from using a scintillator with higher light yield. Thallium-doped CsI [CsI(Tl)] has traditionally been the favored material due to its excellent scintillation properties in combination with the advanced deposition technology available to manufacture the microcolumnar structure of the scintillator film. Materials that are being considered for future application include $\text{Ba}_2\text{CsI}_5(\text{Eu})$ and $\text{LuI}_3(\text{Ce})$. Their light yields are extremely high and studies of appropriate deposition processes are already under way. First results are very promising.

B. Software Upgrades

In order to develop algorithms for the low energy range, data from two radioactive sources, Am-241 (primary emission at 59.54 keV) and Cd-109 (primary emission at 21.99 keV and 22.16 keV) were acquired using the EMCCD in combination with a CsI(Tl) scintillator of $450 \mu\text{m}$ thickness. Both sources were positioned at various distances from the detector during data taking. Different readout rates and settings for on-chip binning were applied during the measurements. Furthermore, both a 1:1 and a 3:1 optical taper were used in various tests to couple the scintillator to the chip of the EMCCD. Before, after and in-between measurements, background data were recorded without the radioactive sources present. An example of a background-subtracted frame can be found in the top left image of Figure 12 for the 256 pixel by 256 pixel sized EMCCD chip. In this specific case the 1:1 taper was in place and 2×2 on-chip binning was applied.

In order to locate events in each acquired data frame accurately, it is useful to smooth the data before centroiding hit locations. After testing and comparing various software filters, the best results were achieved using a spatial bandpass filter to smooth the image. The applied function requires two parameters in addition to the data input: typical object size to be detected and characteristic length scale of noise

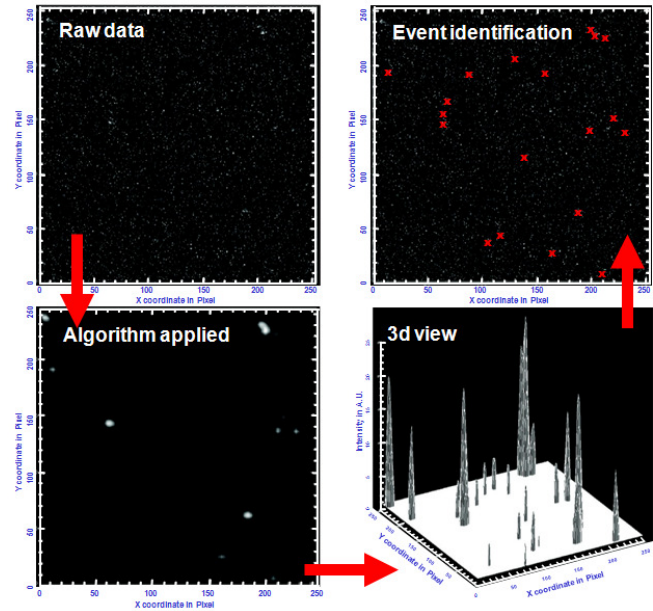


Fig. 12. These four plots illustrate the analysis steps from raw data to single event detection using the algorithms specially developed for this data acquisition mode with the EMCCD detector system.

given in pixels. Applying the bandpass filter to the data frame shown in the upper left plot of Figure 12 yields typically a frame as depicted in the lower left plot of the same figure. The lower right image in Figure 12 demonstrates how a three-dimensional representation of the above smoothed image frame will appear. It is easily seen that the number of detected events by a spot-finding routine will depend not only on the degree of filtering and smoothing but also on the threshold used to distinguish real source events from background hits. Some fine-tuning and testing is required to optimize the software to obtain best results. The software developed to locate events in background-subtracted x-ray data uses a routine locating features of a certain size in each data frame. Generally, this will yield a large number of events which include “real hits” (clusters created by x-ray photons) as well as “fake hits” (clusters that result from background fluctuations and the smoothing routines). Therefore, the brightness of the detected events needs to be taken into account in a second step providing a clear cut that enables the user to distinguish real events from fake ones with very high accuracy. The upper right image of Figure 12 shows the results obtained using the software. The detected events have been plotted on top of the original data frame.

In order to determine how well the code is performing in reproducing the actual number of expected events from each source, an estimate of these numbers based on first principles has been done. In a first order approximation the following features have been accounted for: solid angle of radioactive source with respect to the detector, intensity and branching ratios of the measured sources, losses in the optical taper, efficiency of the scintillator material, and QE of the EMCCD

as well as specific features of the detector housing (e.g. plastic cover). As can be seen in Figure 13, the number of detected events agrees well with expectations for Am-241. For Cd-109 an almost flat distribution is observable instead of the quadratic $1/(distance)^2$ decay. This can be understood as follows: for

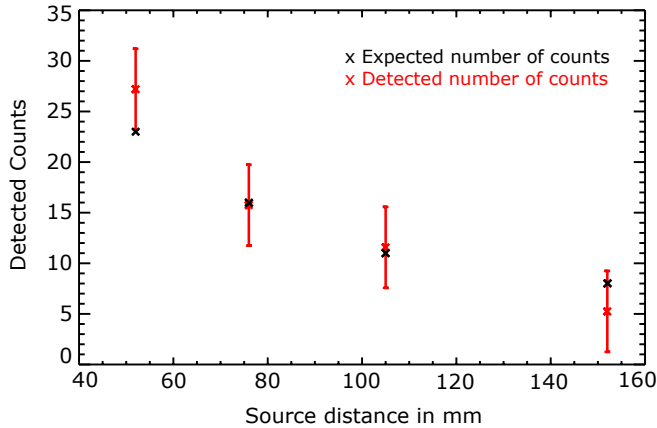


Fig. 13. Comparison of expected and observed counts using single photon detection. The image shows an Am-241 source located at various distances of the detector. The number of expected events is well reproduced by the experimental observations.

americium mostly photons of (relatively) high energy, i.e. 59.54 keV, are expected. The detector in combination with the 450 μ m thick CsI scintillator is perfectly suited for this case. For Cd-109 on the other hand most incident photons will be of lower energy (21.99 keV and 22.16 keV). Only a small fraction of the cadmium-induced events (about 3.6%) are 88.04 keV photons. A thinner scintillator should likely have been used in order to be sensitive to low energy photons around and below 22 keV. The observed events in the case of cadmium can be explained as a combination of real 88 keV events and fake events which are detected mainly due to the fact that the brightness cut in this case is not very efficient.

In summary, we developed and tested an IDL-based code to detect single photon events in data acquired with the RMD detector. Preliminary results indicate that higher energy photons can be detected as expected, while for low energy photons similar results should be achievable using a thinner scintillator. The lower energy threshold however remains yet to be determined. Future work will focus on several tasks. One goal to improve the code used for single photon counting is to make the software more robust. Some improvement in software speed will also be desirable, since this will improve the handling of larger volumes of data. This is important since generally several hundred frames are taken per measurement. This number of frames might even increase (in comparison with operation in integration mode) due to the fact that the count rate per frame is limited since overlapping hits are extremely difficult to detect. An upper limit on the maximal count rate per data frame will be determined along with the low energy threshold achievable for various scintillators. Further work will also improve the determination of deposited energy and thus enhance the energy resolution.

VII. CONCLUSIONS AND OUTLOOK

In this paper, we present results for the first use of a scintillator-EMCCD camera for calibrating hard x-ray telescopes, demonstrated during the ground calibration of the NuSTAR flight optics. The advantages of this detector are multifold and promising. The achievable spatial resolution is excellent, and the turn-key operation simplifies the use of such a detector for calibrating future missions. At the moment, we are enhancing the energy resolution of the detector by developing algorithms to run the detector in single-photon-counting mode. Furthermore hardware upgrades of the EMCCD itself, the scintillator material and the bonding of both by a fiberoptic taper are under investigation. This will render the detector even more suitable for hard x-ray optics calibrations and simplify energy-dependent studies of effective area and PSF. We are confident that our ongoing upgrades of the detector will result in a device highly suitable for calibrations of any future space mission employing hard x-ray optics.

ACKNOWLEDGMENT

This work was performed under the auspices of the U.S. Department of Energy by Lawrence Livermore National Laboratory under Contract DE-AC52-07NA27344. The support of the Laboratory Directed Research and Development Program is gratefully acknowledged. We thank our colleagues at NuSTAR for their support and cooperation and Columbia University for hospitality. We also thank NASA for funding this research under grant number NNX11CH32P.

REFERENCES

- [1] F. A. Harrison *et al.*, "Development of the HEFT and NuSTAR focusing telescopes", *Exp. Astron.*, 20,131-137 (2005).
- [2] B. D. Ramsey *et al.*, "First Images from HERO, a Hard X-Ray Focusing Telescope", *ApJ*, 568, 432-435 (2002).
- [3] J. Tueller *et al.*, "InFOCUS Hard X-Ray Imaging Telescope", *Exp. Astron.*, 20, 121-129 (2005).
- [4] F. A. Harrison *et al.*, "The Nuclear Spectroscopic Telescope Array (NuSTAR)", *Proceedings of SPIE*, 7732:77320S (2010).
- [5] T. Takahashi *et al.*, "The ASTRO-H Mission", *Proceedings of SPIE*, 7732:77320Z (2010).
- [6] http://www.andor.com/scientific_cameras/ixon_emccd_camera/
- [7] V. V. Nagarkar *et al.*, "Fast X-Ray/ γ -Ray Imaging using Electron Multiplying CCD-Based Detector", *NIM A*, 563, 45-48 (2006).
- [8] V. V. Nagarkar *et al.*, "Structured CsI(Tl) Scintillators for X-Ray Imaging Applications", *IEEE Trans Nucl. Sci.*, 45, 3, 492-496 (1998).
- [9] C. J. Hailey *et al.*, "The Nuclear Spectroscopic Telescope Array (NuSTAR): Optics Overview and Current Status", *Proceedings of SPIE*, 7732:77320T (2010).
- [10] W. Craig *et al.*, "Fabrication of the NuSTAR Flight Optics", *Proceedings of SPIE*, 8147, 81470H (2011).
- [11] J. Koglin *et al.*, "First Results from the Ground Calibration of the NuSTAR Flight Optics", *Proceedings of SPIE*, 8147, 81470J (2011).
- [12] G. Pareschi *et al.*, "Design and Development of the Optics System for the NHXM Hard X-Ray and Polarimetric Mission", *Society of Photo-Optical Instrumentation Engineers (SPIE) Conference Series*, 7437 (2009).
- [13] F. Christensen *et al.*, "Coatings for the NuSTAR Mission", *Proceedings of SPIE*, 8147, 81470U (2011).
- [14] N. F. Brehnholt *et al.*, (NuSTAR Optics Team), "The Rainwater Memorial Calibration Facility for X-Ray Optics", *X-Ray Optics and Instrumentation*, 2011, 285079 (2011).
- [15] A. Zoglauer *et al.*, "Simulating Extended Galactic Sources with the NuSTAR Simulator NuSIM", *BAAS*, Vol 43, No. 6, 43.07 (2011).